Plant Mol Biol (2015) 87:17–30
DOI 10.1007/s11103-014-0257-y

A SNP in *OsMCA1* responding for a plant architecture defect by deactivation of bioactive GA in rice

Zhenwei Liu · Qin Cheng · Yunfang Sun · Huixia Dai · Gaoyuan Song · Zhibin Guo · Xuefeng Qu · Daiming Jiang · Chuan Liu · Wei Wang · Daichang Yang

Received: 13 August 2014 / Accepted: 8 October 2014 / Published online: 12 October 2014

Abstract Plant architecture directly affects biomass in higher plants, especially grain yields in agricultural crops. In this study, we characterized a recessive mutant, *plant architecture determinant* (*pad*), derived from the *Oryza sativa* ssp. *indica* cultivar MH86. The mutant exhibited severe dwarf phenotypes, including shorter and stunted leaves, fewer secondary branches during both the vegetative and reproductive growth stages. Cytological studies revealed that *pad* mutant growth defects are primarily due to the inhibition of cell expansion. The *PAD* gene was isolated using a map-based cloning strategy. It encodes a plasma membrane protein OsMCA1 and a SNP responsible for a single amino acid change was found in the mutant. *PAD* was universally expressed in rice tissues from the vegetative to reproductive growth stages, especially in seedlings, nodes and rachillae. Quantitative real-time PCR analysis revealed that the most of the genes responding to gibberellin (GA) metabolism were up-regulated in *pad* mutant internodes. The endogenous GA content measurement revealed that the levels of GA_1 were significantly decreased in the third internode of *pad* mutants. Moreover, a GA response assay suggested that *OsMCA1/PAD* might be involved in the regulation of GA metabolism and signal transduction. Our results revealed the *pad* is a loss-of-function mutant of the *OsMCA1/PAD*, leading to upregulation of genes related to GA deactivation, which decreased bioactive GA levels.

Keywords Internode elongation · GA biosynthesis · GA deactivation · Map-based cloning · Plant architecture · Plant height · Rice *pad* mutant

Electronic supplementary material The online version of this article (doi:10.1007/s11103-014-0257-y) contains supplementary material, which is available to authorized users.

Z. Liu · Q. Cheng · Y. Sun · H. Dai · G. Song · Z. Guo · X. Qu · D. Jiang · C. Liu · W. Wang · D. Yang (✉)
State Key Laboratory of Hybrid Rice, College of Life Sciences, Wuhan University, Luojia Hill, Wuhan 430072, Hubei Province, China
e-mail: dyang@whu.edu.cn

Introduction

Plant architecture directly affects grain yields. Rice plant architecture, which has recently been extensively investigated (Sakamoto and Matsuoka 2004; Springer 2010; Wang and Li 2005, 2008; Xing and Zhang 2010; Yang and Hwa 2008; Zhang et al. 2008), is a complicated agronomic trait that is mainly determined by tiller number, tiller angle, leaf arrangement, plant height and panicle morphology. In previous studies, several genes involved in controlling the above-mentioned components, such as *TEOSINTE BRANCHED 1* (*OsTB1*), *MONOCULM 1* (*MOC1*), *LAZY1* (*LA1*), *Tiller Angle Control 1* (*TAC1*), *PROSTRATE GROWTH 1* (*PROG1*), *YABBY1* (*YAB1*), OsDWARF4, *Loose Plant Architecture1* (*LPA1*), *Semi-Dwarf1* (*SD1*) and *SOUAMOSA PROMOTER BINDING PROTEIN-LIKE 14* (*OsSPL14*), were identified based on natural and artificially generated mutants of various rice varieties (Dai et al. 2007; Jiao et al. 2010; Jin et al. 2008; Li et al. 2007; 2003; Miura et al. 2010; Sakamoto et al. 2006; Sasaki et al. 2002; Takeda et al. 2003; Tan et al. 2008; Wu et al. 2013; Yoshihara and Iino 2007; Yu et al. 2007). Plant height, an important trait that affects plant architecture, is determined by the number and lengths of internodes as well as environmental conditions (Wang and Li 2005). Plant height is primarily regulated by autologous phytohormones, including gibberellins (GAs) and brassinosteroids (BRs; Yang and Hwa 2008).

The GA plant hormones, whose major active forms include GA_1 and GA_4, are involved in plant height determination. The GAs is consisted of a large family of tetracyclic diterpenoid carboxylic acids and functions in diverse aspects of plant growth and development, especially internode elongation (Sakamoto 2006; Sakamoto and Matsuoka 2004). In recent years, the mechanisms of GA metabolism have been elucidated (Olszewski et al. 2002; Thomas et al. 2005; Yamaguchi 2008). Bioactive GAs are first synthesized from geranylgeranyl diphosphate (GGDP), which is a common diterpene precursor. GGDP is then converted to GA_{12} via a series of intermediates by four enzymes, *ent*-copalyl diphosphate (CDP) synthase (CPS), *ent*-kaurene synthase (KS), *ent*-kaurene oxidase (KO) and *ent*-kaurenoic acid oxidase (KAO). As an important checkpoint in the GA biosynthesis pathway, GA_{12} is converted to GA_{53} by undergoing 13-hydroxylation by GA13-oxidase (GA13ox; Magome et al. 2013). Then, GA_{53}/GA_{12} is converted to GA_{20}/GA_9 by 2-oxoglutarate–dependent dioxygenase (ODD) GA20ox (GA20-oxidase) through two parallel pathways in a three- or four-step process. In the final step of bioactive GA synthesis, GA_{20} and GA_9 are converted to GA_1 and GA_4, respectively, by ODD GA3-oxidase (GA3ox). In addition, GA_1/GA_4 and GA_{20}/GA_9 are deactivated by ODD GA2-oxidases (GA2oxs) and a cytochrome P450 monooxygenase (CYP714D1/EUI; Zhu et al. 2006). These genes have also been identified based on the corresponding GA-deficient mutants in rice (Sakamoto et al. 2004).

GA homoeostasis is controlled through negative feedback regulation of GA biosynthetic enzymes and positive feed-forward regulation of GA catabolic enzymes meditated by the GA signaling pathway (Hedden and Thomas 2012; Yamaguchi 2008). In plants harboring related gain-of-function mutations in repressors or loss-of-function mutations in components of positive regulation, the levels of bioactive GAs or GA biosynthetic gene expression are highly elevated. Loss-of-function mutations in repressors result in lower levels of bioactive GAs or GA20ox and GA3ox mRNAs compared with those of wild type (WT; Olszewski et al. 2002).

In the present study, a natural mutant of the rice *indica* variety Minghui 86 (MH86), *pad*, exhibited a visibly abnormal phenotype that consisted of reduced plant height, shorter and stunted leaves, fewer secondary branches, lower seed set and higher tiller numbers compared with WT (MH86). We cloned the *pad* gene using a map-based cloning strategy and found that it is encoded by *OsMCA1,* a homolog of *AtMCA1* in *Arabidopsis*. A nucleotide substitution in the kinase domain was identified in the mutant. The *OsMCA1/PAD* gene is constitutively expressed throughout the whole plant and is highly expressed in seedling, leaf, young leaf, internode and young panicle tissues. Further studies indicated that the *OsMCA1/PAD* gene is involved in rice plant architecture and substantially affects rice plant height by regulating GA metabolism.

Materials and methods

Plant materials

The rice mutant *plant architecture determinant*, *pad*, was identified from the *O. sativa* ssp. *indica* cultivar Minghui 86. All rice plants were planted in a field in Wuhan during the natural growing season.

Histological analysis

For microscopy studies, leaves and the uppermost internodes at the appropriate developmental stage were harvested, fixed in fixation solution (4 % paraformaldehyde (Sigma, Ronkonkoma, NY, USA) in 1× PBS, 0.02 % KCl, 0.8 % NaCl, 0.178 % $Na_2HPO4{\cdot}2H_2O$, 0.024 % KH_2PO_4 and 0.1 % Triton X-100) overnight and sequentially dehydrated in 25, 50, 70, 80, 90, 95 and 100 % ethanol for 5 min each. Then, the dehydrated material was embedded in Steedman's wax (polyethylene glycol 400 distearate: 1-hexadecanol; 9:1) and sectioned using a microtome to a thickness of 8 μm. The sections were adhered to slides coated with poly-L-lysine and then sequentially de-waxed in 100, 95, 80, 50 and 30 % ethanol for 5 min each. Finally, the sections were visualized and photographed on an inverted phase contrast microscope (IX51; Olympus).

Genetic analysis and map-based cloning

An F2 population derived from the *pad* mutant crossed with Nongken58 (*japonica*) was used for genetic linkage analysis and fine mapping. In total, 200 polymorphic SSR markers were identified from 600 SSR primer pairs used to screen the parents. Bulk Segregant Analysis (BSA) was used to assess SSR marker linkage to *pad* and roughly map the *pad* locus to chromosome 3. SNP markers were obtained by sequencing the region of interest. Finally, the *pad* locus was narrowed down to an 8.7-kb region between two SNP markers, S2 and S3, through 477 and 3,869 homozygous recessive individuals from the F2 population of the *pad* mutant × NK58, respectively. The candidate gene was identified by sequencing the genomic DNA in this region from the *pad* mutant and WT plants and generating pairwise sequence alignments using MacVector.

Plasmid construction

The coding region of the candidate gene was confirmed by comparing the sequence of the genomic DNA fragment with

information in the GenBank, UniProtKB and Gramene databases. A 2,945-bp fragment containing 1,688 bp of upstream sequence and the 1,257 bp CDS was synthesized by GeneScript (Nanjing, China) and cloned into the binary vector *pCAMBIA1300*. The construct was then transformed into *Agrobacterium* strain EHA105 and designated *pOsPMP618*.

For the construction of the *GFP-OsMCA1* fusion plasmid, the full-length *OsMCA1* coding sequence was fused to the C terminus of the GFP coding sequence without a termination codon to create an in-frame fusion. The fragment was then cloned into a transient expression vector (*pOsPMP550*) under the control of the CaMV 35S promoter. The resulting plasmid was designated *pOsPMP622*.

For the construction of the *OsMCA1-GUS* fusion vector, an approximately 1.69 kb promoter region from the *OsMCA1* gene was amplified and cut with *HindIII* and *NaeI*. The sequence was then inserted upstream of the 5′ end of the *uidA* gene encoding β-glucuronidase (GUS) in the binary vector *pCAMBIA1300* to create the resulting plasmid, which was designated *pOsPMP617*.

Plant transformation

For the rescue of the *pad* mutant, the *pOsPMP618* construct was introduced into calli derived from the *pad* mutant by *Agrobacterium*-mediated transformation. All transgenic rice plants were identified by PCR using the primer pair 618-1-F and 618-1-R (Supplemental Table S1). All transgenic plants were grown in a greenhouse at the Wuhan University Campus. For all *Agrobacterium*-mediated transformations, the plasmids were introduced into the *Agrobacterium* strain EHA105.

Tissue-specific analysis

For the tissue-specific expression of *OsMCA1, pOsPMP617* was introduced into the *japonica* rice variety Nongken58, and positive transgenic plants were identified by PCR using the primer pair GUS-F and GUS-R (Supplemental Table S1). GUS activities were analyzed in situ according to a method described previously (Jefferson 1989). Briefly, tissues from the transgenic plants were washed in staining buffer containing 50 mM $NaPO_4$ buffer (pH 7.0), 2 mM $K_3Fe(CN)_6$, 2 mM $K_4Fe(CN)_6$ and 0.2 % Triton X-100 three times on ice and then incubated in staining buffer supplemented with an X-Gluc stock solution (1 mM) at 37 °C overnight. GUS-stained tissues were observed on a stereo microscope and photographed with a camera (EOS 400D; Canon).

Transient assay on epidermal cells

The GFP alone (*pOsPMP623*) and *GFP-OsMCA1* (*pOsPMP622*) fusion constructs were introduced into onion epidermal cells by particle bombardment using a PDS-1000/He (BIO-RAD). After incubation for 18–24 h at 26 °C, GFP fluorescence was observed on an inverted phase contrast microscope (IX51; Olympus).

Phylogenetic analysis

The putative homologs of OsMCA1 were identified using the Basic Local Alignment Search Tool from the National Center for Biotechnology Information (http://blast.ncbi.nlm.nih.gov/Blast.cgi). A phylogenetic tree of OsMCA1 homologs was constructed using the neighbor-joining (NJ) function of MEGA 5.2. The number of bootstrap replicates was estimated at 1,000, and all sites with alignment gaps/missing sequences in pairwise sequence comparisons were deleted.

RNA extraction and quantitative RT-PCR

All rice tissues were harvested, immediately frozen in liquid nitrogen and stored at −80 °C until use. Total RNA was extracted using TRIzol Reagent (Invitrogen, Carlsbad, CA, USA) according to the manufacturer's instructions and then was treated with RNase-free DNase I (New England Biolabs, Hitchin, UK) to remove DNA contamination prior to cDNA synthesis. First-strand cDNA synthesis was performed using M-MLV reverse transcriptase (Promega, Madison, USA) using 2–3 μg of RNA template and an oligo (dT) primer.

Quantitative RT-PCR was performed on a StepOne System (ABI) using the following program: 95 °C for 10 min followed by 40 cycles of 95 °C for 10 s and 60 °C for 30 s and a melting curve from 60 °C to 95 °C in 0.7 °C increments. Relative gene expression levels were calculated via the ΔΔCT method, and the rice *Actin1* gene was used as an internal control to normalize the data. The primers used for qRT-PCR analysis are listed in Supplemental Table S1. All analyses were performed in triplicate. The transcripts of *EUI1* were detected by Semi quantitative RT-PCR as described previously (Zhu et al. 2006). The rice *Actin1* gene was used as an internal control with the prime pair as described previously (Huang et al. 2010).

Exogenous GA effects and GA content analysis

Exogenous GA treatment of rice seedlings was performed as described in (Ikeda et al. 2001) with minor modifications. Briefly, 15 seeds from WT and *pad* plants were surface sterilized for 30 min in a 2 % NaClO solution and washed four times with sterile distilled water. The sterilized seeds were soaked in sterile distilled water with or without 6.85 μM uniconazol for 36 h. The pretreated seeds were

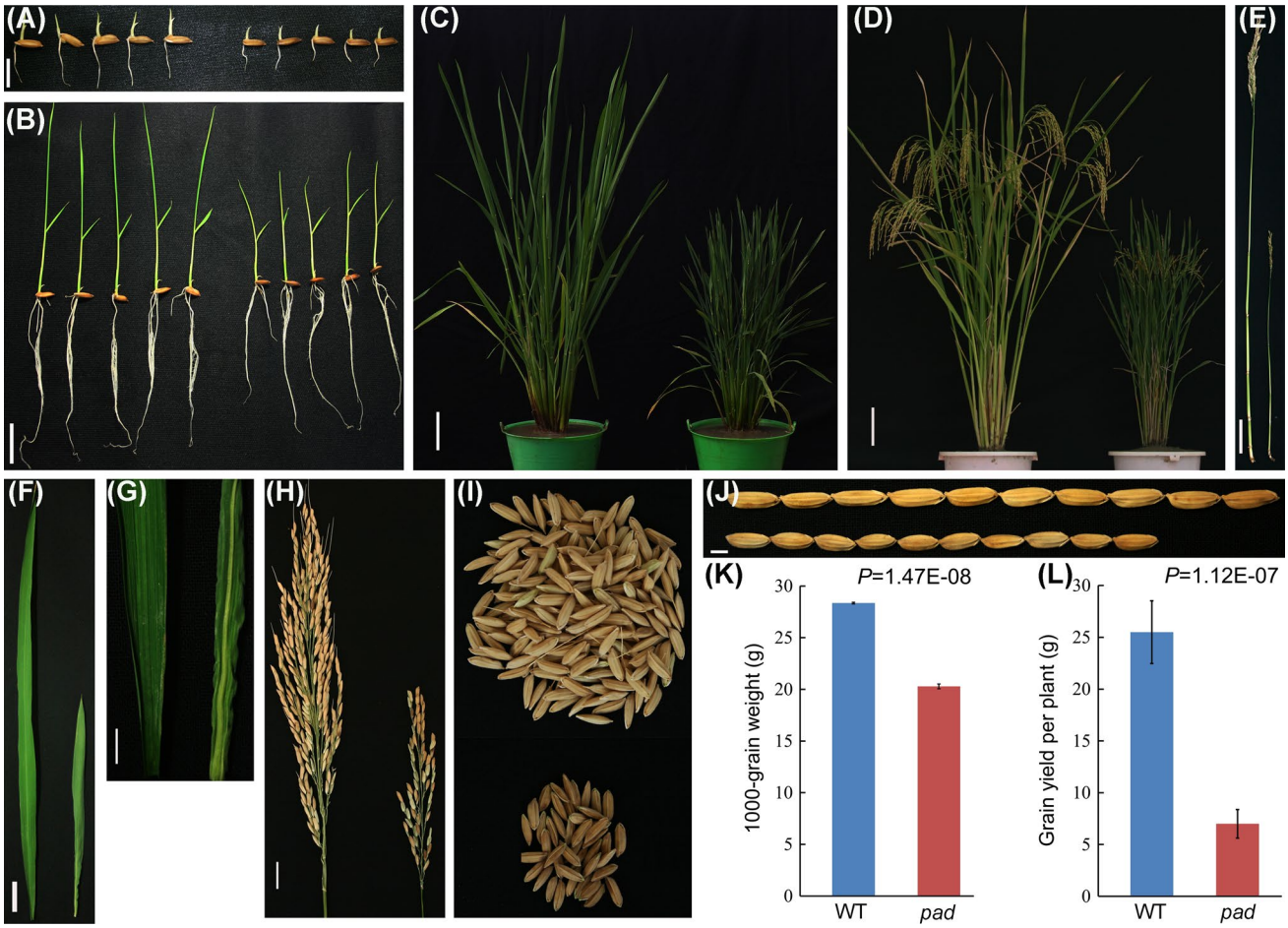

Fig. 1 Morphological characterization of the *pad* mutant. **a** Seed germination of WT (*left*) and *pad* (*right*) after 2 days. **b** WT (*left*) and *pad* (*right*) seedlings 6 days after germination. **c** WT (*left*) and *pad* (*right*) rice plants before heading. **d** WT (*left*) and *pad* (*right*) rice plants after grain filling. **e** Plant height of WT (*left*) and *pad* (*right*). **f** Leaf morphology of WT (*left*) and *pad* (*right*). **g** Morphology of the leaf base of WT (*left*) and *pad* (*right*). **h** Panicle of WT (*left*) and *pad* (*right*). **i** Grains per main panicle from WT (*top*) and *pad* (*bottom*). **j** Comparison of grain lengths between WT (*top*) and *pad* (*bottom*). **k** 1,000-grain weight and **l** grain yield per plant from WT and *pad*. The data are given as the mean ± SD (n = 8–15) in (**j**). The mean ± SD was calculated from three biological replicates and values were determined by the Student's *t* test in **k** and **l**. *Bars* 1 cm in **a**; 2 cm in **b** and **f**–**h**; 10 cm in **c**–**e**; 3 mm in **j**

immersed in sterile distilled water for 24 h. Finally, the seeds were placed on 1 % agar plates supplemented with GA_3 at different final concentrations ranging from 0.01 to 100 μM and grown at 26 °C under continuous light. After approximately 8 days, the length of the second leaf sheath was measured.

For GA content analysis, the individual internodes, including the uppermost internodes to the third internodes of WT plants and *pad* mutants, were harvested at the stage when the uppermost and second internodes were elongating and were immediately frozen in liquid nitrogen and stored at −80 °C until GA extraction. The endogenous GAs were detected by nano-LC–ESI-Q-TOF–MS analysis as described previously (Chen et al. 2012). All measurement were conducted three times.

Results

A *pad* mutant exhibits plant architecture defects

We identified a natural mutant of the *O. sativa* ssp. *indica* variety MH86 with plant architecture defects. This mutant exhibits a visibly abnormal phenotype during the vegetative and reproductive growth stages compared with WT. During growth and developmental stages, the mutant showed shorter root, smaller shoot and leaf sizes and reduced height (Fig. 1a–c). These mutated phenotypes, especially, became more apparent in the stem elongation stage to the seed setting stage (Fig. 1d). Compared with WT plants, the leaf length and plant height of the mutants were decreased by 59.16 % (17.90 ± 0.52 cm in the mutant

Table 1 Comparison of the agricultural traits of *pad* and WT (MH86)

Trait	PH (cm)	PL (cm)	SN	SF (%)	TN	GNP	NPB	NSB	GL (mm)	GW (mm)	GT (mm)
WT	126.3 ± 6.4	29.3 ± 1.1	251.8 ± 19.5	81.9 ± 3.0	7.5 ± 1.2	1,099.7 ± 134.5	10.7 ± 0.5	44.8 ± 4.8	9.99 ± 0.36	2.98 ± 0.09	2.05 ± 0.08
pad	67.1 ± 3.8	13.1 ± 0.5	69.7 ± 10.7	49.9 ± 4.5	18.2 ± 3.0	734.0 ± 102.8	7.1 ± 0.7	1.3 ± 1.0	9.07 ± 0.26	2.92 ± 0.07	1.86 ± 0.08
P value	2.04E−165	1.04E−11	2.05E−09	4.58E−08	3.74E−09	3.52E−04	8.26E−16	1.57E−23	2.90E−12	0.02	5.46E−10

All data are given as the mean ± SD and significant differences were determined by the Student's *t* test

PH plant height, *PL* panicle length, *SN* spikelet number per panicle, *SF* spikelet fertility, *TN* tiller number, *GNP* grain number per plant, *NPB* number of primary branches per panicle, *NSB* number of secondary branches per panicle, *GL* grain length, *GW* grain width, *GT* grain thickness

vs. 43.83 ± 2.02 cm in WT; $P < 0.001$) and 46.87 % (67.1 ± 3.8 cm in the mutant vs. 126.3 ± 6.4 cm in WT; $P < 0.001$), respectively (Fig. 1e, f; Table 1). Moreover, the leaves of the mutant were curly and wrinkled with abnormal rachis from the base of the leaf (Fig. 1g).

Furthermore, panicle size, spikelet number per panicle, grain length, 1,000-grain weight and seed set were obviously affected in the mutant (Fig. 1h–k; Table 1). The number of primary branches was significantly decreased by 33.73 % in the mutant compared with the WT (7.1 ± 0.7 in the mutant vs. 10.7 ± 0.5 in WT; $P < 0.001$), and the secondary branch number was also lower in the *pad* mutant (1.3 ± 1.0 in the mutant vs. 44.88 ± 4.8 in WT; $P < 0.001$; Table 1). In addition, the mutant exhibited a significant decrease in grain number per plant and grain size compared with WT (Table 1). Grain length and thickness were significantly reduced in the mutant (Fig. 1j; Table 1), whereas grain width was not affected. Compared with WT, 1,000-grain weight and grain yield per plant in the mutant were significantly decreased by 39.79 % (20.28 ± 0.24 g in the mutant vs. 28.35 ± 0.09 g in the WT; $P = 1.47E{-}08$) and 72.55 % (7.00 ± 1.38 g in the mutant vs. 25.50 ± 3.03 g in the WT; $P = 1.12E{-}07$), respectively (Fig. 1k, l). These results demonstrate that this mutation strongly affects rice plant architecture and in turn, grain yield. Therefore, we designated this mutant *pad*.

Cloning of the *PAD* gene through a map-based cloning approach

Genetic analysis of the *pad* mutant indicated that the phenotype of the F1 plants was WT. In the F2 population of MH86 × *pad*, 30 individuals exhibited a mutant phenotype out of 112 individuals ($\chi^2(3{:}1) = 0.19$, $P = 0.663 > 0.5$), fitting Mendel's single gene segregation. These data indicate that *pad* mutant phenotypic traits are controlled by a single recessive locus.

To genetically map the *pad* gene, an F2 population of *pad* × Nongken 58 was subjected to a map-based cloning approach. A total of 80 polymorphic simple sequence repeat (SSR) markers distributed across 12 chromosomes were available for genetic analysis. The *pad* locus was mapped to the long arm of chromosome 3 by BSA (Fig. 2a). To fine map the *pad* locus, a large F2 population of 2,000 plants and nine polymorphic SSR markers flanking the region of the *pad* locus were used. A total of 25 homozygous recessive plants with mutant phenotypes were screened and used for further analysis. The *pad* locus was flanked by two SSR markers, RM22 and RM14491 (Fig. 2a). To further delimit the locus, a total of 470 homozygous recessive plants were screened and analyzed using four polymorphic SSR markers, RM 6301, RM14390, RM14400 and RM6883. The *pad* locus was mapped to the region between the SSR

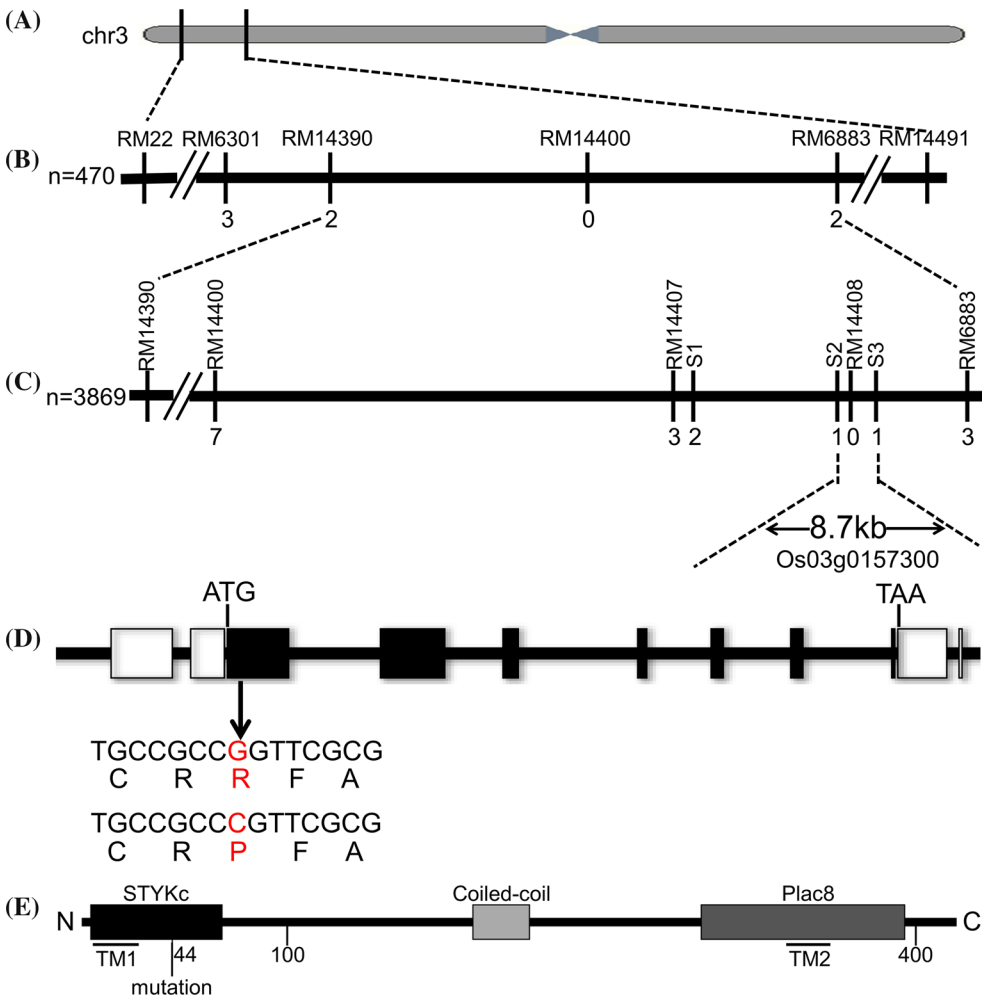

Fig. 2 Map-based cloning of the *PAD* gene. **a** The *pad* locus was mapped to chromosome 3. **b** The *pad* locus was further delimited to the region between two SSR markers, RM14390 and RM6883. The number under each marker represents the number of recombination events. **c** The *pad* locus was finally determined to fall within an 8.7-kb region flanked by two SNP markers, S2 and S3. **d** Schematic of the *pad* gene structure. Exons and introns are indicated by *black boxes* and *lines*, respectively. *White boxes* represent the 5′ and 3′ untranslated regions. The position of the mutation in *pad* is indicated by an arrow. **e** Schematic representation of the predicted domains of OsMCA1/PAD and the position of the mutation in the pad mutant. The *black box* indicates the SYTKc domain. The *light grey box* indicates the coiled–coil domain. The *dark grey box* indicates the PLAC8 domain. The *bars* indicate the positions of the potential transmembrane segments (TMs)

markers RM14390 and RM6883 with a physical distance of 387.79 kb based on the recombination frequency (Fig. 2b). To further localize the *pad* gene, another four polymorphic SSR markers, RM14400, RM14407, RM14408 and RM6883, were used to screen 3,869 homozygous recessive individuals, delimiting the *pad* locus to a region between RM14407 and RM6883 with a physical distance of 52 kb (Fig. 2c). To accurately determine the causative gene of the *pad* phenotype from this 52 kb region, we identified three SNPs within this region, S1, S2 and S3, based on sequences available in rice genomic databases. Finally, the *pad* locus was determined to fall within an 8.7 kb region flanked by the markers S2 and S3 located on a bacterial artificial chromosome contig, OSJNBa0011L14 (Fig. 2c). Only one open reading frame (ORF), *Os03g0157300*, was found in this region. Sequencing of the genomic DNA in this region revealed that the mutant allele harbored a G to C substitution at nucleotide position 131 in the predicted exon 2 of *Os03g0157300* (Fig. 2d). Further sequencing of the different recombinant individuals verified that this SNP was completely linked to the *pad* locus; therefore, this gene was considered the candidate gene in the *pad* mutant. Further comparisons found that the single nucleotide substitution produced the amino acid change R44P (Fig. 2d, e; Supplemental Fig. S1). *Os03g0157300* is predicted to encode *Mid1-complementing activity1*, *OsMCA1*, which is a homolog of *AtMCA1* and *AtMCA2* in *Arabidopsis* (Kurusu et al. 2012; Nakagawa et al. 2007).

Bioinformatic analysis using the Simple Modular Architecture Research Tool (http://smart.embl-heidelberg.de/smart/job_status.pl?jobid=581912666854831383877959oJYXLFqQqK) indicated that the OsMCA1/PAD protein comprises a STYKc domain at the N terminus, a coiled-coil region in the middle and a PLAC8 motif at the C terminus (Fig. 2e; Supplemental Fig. S2). Two putative transmembrane segments (TM1 and TM2) are predicted by the SOSUI system (http://bp.nuap.nagoya-u.ac.jp/sosui/cgi-bin/adv_sosui.cgi). TM1 lies in the STYKc domain, and TM2 locates in the PLAC8 motif (Fig. 2e; Supplemental Fig. S2).

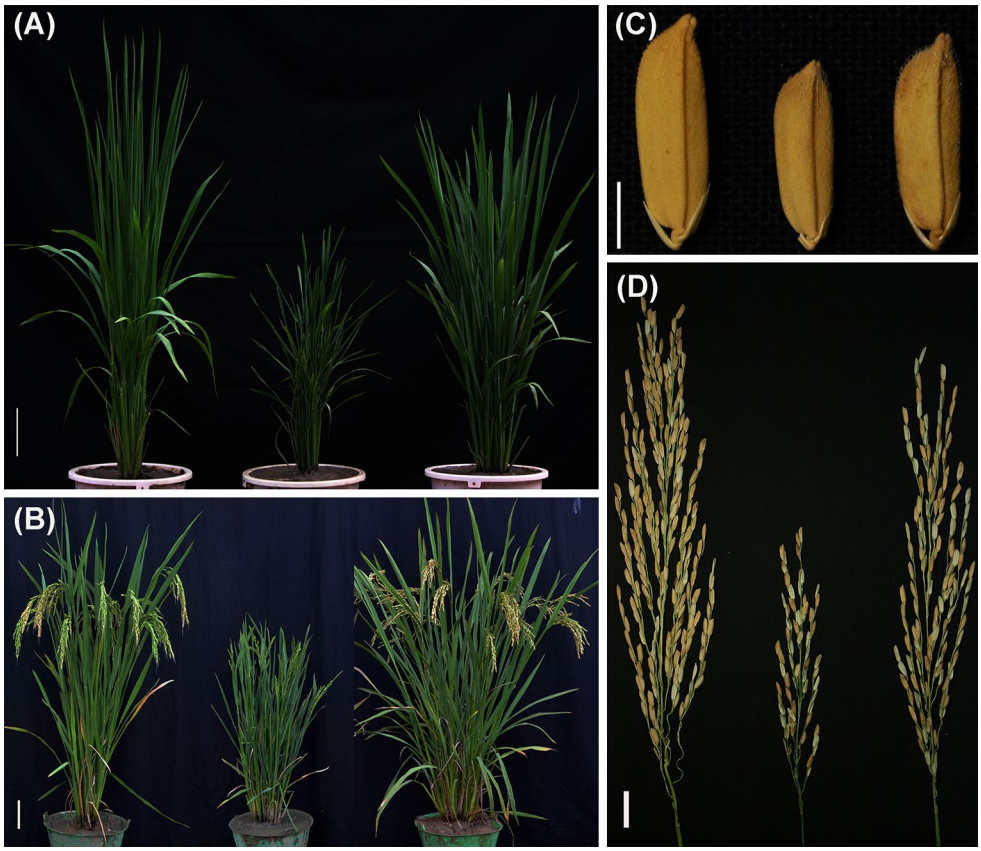

Fig. 3 Genetic complementation of the *pad* mutant. Transgenic rice morphology at the vegetative stage (**a**) and the mature stage (**b**). **c** Grain size of transgenic rice. **d** Panicle morphology at the mature stage. WT (*left*), the *pad* mutant (*middle*) and a genetic complementation line (*right*) are shown. *Bars* 10 cm in (**a**) and (**b**); 3 cm in (**c**); 2 cm in (**d**)

Genetic complementation for the *pad* phenotype

To confirm that *OsMCA1* corresponds to the *pad* locus, we artificially synthesized the *OsMCA1* based on the cDNA sequence of the annotated OsMCA1 polypeptide from the Gramene database (http://ensembl.gramene.org/Oryza_sativa/Info/Index). We amplified the native promoter region and the 5′ untranslated region (UTR), from WT genome and fused into synthetic gene of *OsMCA1,* and then cloned into the binary vector *pCAMBIA1300*. A total of 27 independent transformants were obtained via *Agrobacterium*-mediated transformation into the mutant background. As shown in Fig. 3, all T1 transgenic lines exhibited normal plant architecture (Fig. 3a–d). The genetic complementation experiment demonstrated that the expression of *OsMCA1* gene in mutant background corrects the mutant phenotypes.

The *OsMCA1/PAD* gene is constitutively expressed in rice plants

To investigate the tissue-specific expression profile of the *OsMCA1/PAD* gene during rice development, we performed qRT-PCR analyses on total RNA extracted from various tissues from WT (MH86) and the mutant. In accordance with the expression pattern observed previously, *OsMCA1/PAD* was constitutively expressed in all tissues (Kurusu et al. 2012). In addition, the expression of *OsMCA1/PAD* was significantly decreased in mature, young leaf and seedling tissues in the *pad* mutant compared with WT (Fig. 4a). Conversely, higher expression levels in stems were observed in the *pad* mutant compared with WT, suggesting that *OsMCA1/PAD* may play different roles in leaves and stems. The decrease in *OsMCA1/PAD* gene expression in leaves and the increase in stems are consistent with the curly, wrinkled leaves and reduced plant height in the mutant.

To further understand the tissue specificity of *OsMCA1/PAD* expression in rice, a GUS reporter construct driven by a native promoter was generated and transformed into the rice variety NK58 via *Agrobacterium*-mediated transformation. GUS expression was detected in all tissues throughout the developmental stages (Fig. 4b–j), which was consistent with the previous results and showed the similar expression pattern of *AtMCA2* in *Arabidopsis* (Kurusu et al. 2012; Yamanaka et al. 2010). However, strong expression was found in nodes, inflorescences, young florets and rachillae (Fig. 4f–i), implying that *OsMCA1/PAD* could function in the elongation of nodes and the cell development necessary for plant height and smaller grains, which is consistent with the plant architecture defect in the *pad* mutant.

To determine the subcellular distribution of OsMCA1/PAD, a transient assay was performed. The fluorescent signal from the GFP-OsMCA1 fusion was only detected in the

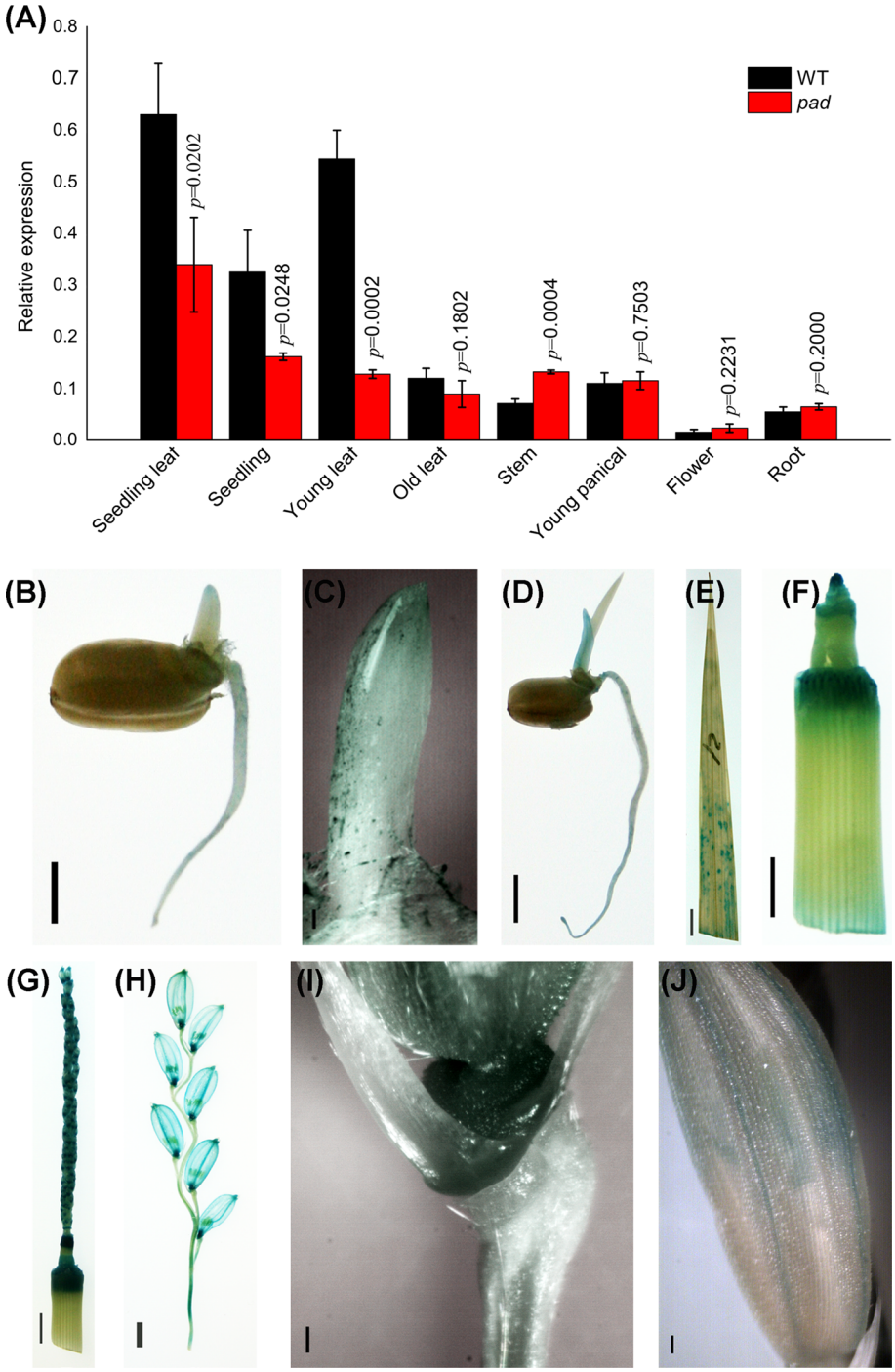

Fig. 4 Expression pattern of *OsMCA1/PAD*. **a** qRT-PCR analysis of *OsMCA1/PAD* in seedling leaf, whole seedling, young leaf (at the tillering stage), old leaf (at the heading stage), stem, young panicle, flower and root tissues. The mean ± SD were calculated from three biological replicates and values were determined by the Student's *t* test. **b–j** GUS analysis of *OsMCA1/PAD* expression; **b** seedlings 2 days after germination; **c** shoot apex of the seedlings 2 days after germination; **d** seedling 4 days after germination; **e** leaf morphology at the vegetative stage; **f** stem at the booting stage; **g** inflorescence; **h** young florets; **i** rachilla; **j** grain husk. *Bars* 2 mm in (**b**); 100 μm in (**c**) and (**i**); 3 mm in (**d**) and (**f–h**); 5 mm in (**e**); 200 μm in (**j**)

plasma membrane (Fig. 5d–f), whereas GFP alone exhibited no obvious subcellular distribution (Fig. 5a–c). This result is consistent with *OsMCA1* encoding a membrane protein (Kurusu et al. 2012).

OsMCA1/PAD affects cell elongation in stems and roots

Based on the expression pattern of *OsMCA1* and the *pad* mutant phenotype, *OsMCA1/PAD* may affect plant architecture. To further investigate whether *OsMCA1/PAD* regulates cell elongation or division, we examined cell morphology in the leaves, the roots of 7-day-old seedling and the uppermost internode at the early stage of heading. Cytological studies revealed that the cell sizes in the leaves and roots of the *pad* mutant were smaller than in those of WT (Fig. 6a, b). In particular, the uppermost internode was significantly longer in WT than that in the mutant (Fig. 6c), which is consistent with the reduced plant height

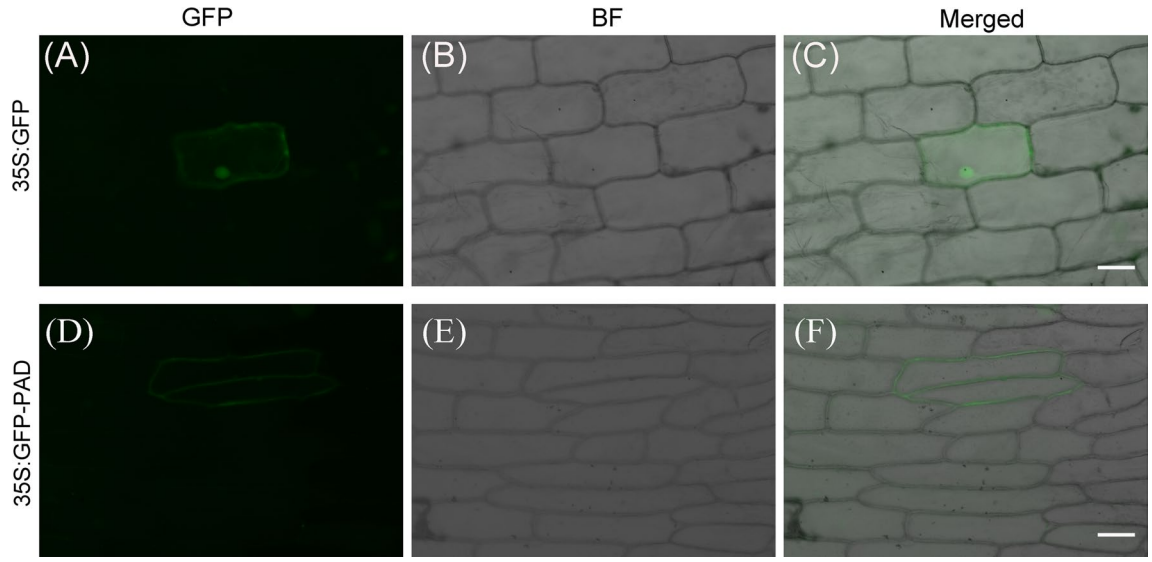

Fig. 5 Cellular localization of OsMCA1/PAD. **a–c** Localization of 35S:GFP in onion epidermal cells. **d–f** Localization of 35S:GFP-OsMCA1 in onion epidermal cells. *Bars* 10 μm

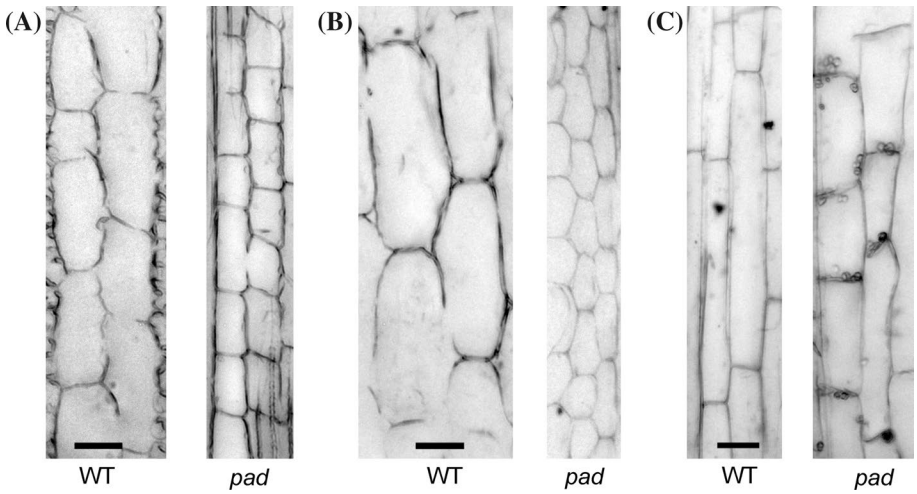

Fig. 6 Longitudinal section analysis of WT and *pad*. **a** Leaf blade from WT and *pad* at the 7-day-old seedling stage; **b** roots from WT and *pad* at the 7-day-old seedling stage; **c** uppermost internodes from WT and *pad* at the heading stage. *Bars* 100 μm

in the mutant (Fig. 1e; Table 1). Taken together, these findings suggest that cell expansion is severely disrupted in the mutant.

OsMCA1/PAD is involved in the regulation of GA metabolism

To categorize the internode elongation pattern of *pad* mutant, we measured the length of each internode in WT and the *pad* mutant. We found that internode elongation in the mutant was greatly restrained. As shown in Fig. 7a, the length from the uppermost to sixth internodes in the *pad* mutant was significantly reduced compared with WT. Furthermore, we found the length of each internode was uniformly reduced in the *pad* mutant. The internode elongation pattern of *pad* mutant presented as the same pattern as WT (Supplemental Fig. S3). This result suggested that the *pad* is a typical dn-type dwarf mutant (Takeda 1979). Moreover, the pattern is also similar to that of some GA-related dwarf mutants (Itoh et al. 2004), implying *pad* could be related to GA metabolism. These results were consistent with cytological studies and indicate that the decreased internode length in the *pad* mutant occurred mainly due to restrained cell elongation in the internodes (Fig. 6c). It simultaneously excludes the *pad* mutant belongs to BR-related dwarf mutant. According to the internode elongation pattern and the dwarf phenotype in the *pad* mutant, which are similar to some rice dwarf mutants that exhibit altered GA responses (Guo et al. 2013; Sakamoto et al. 2004; Ueguchi-Tanaka et al. 2000). Therefore, we hypothesize that the

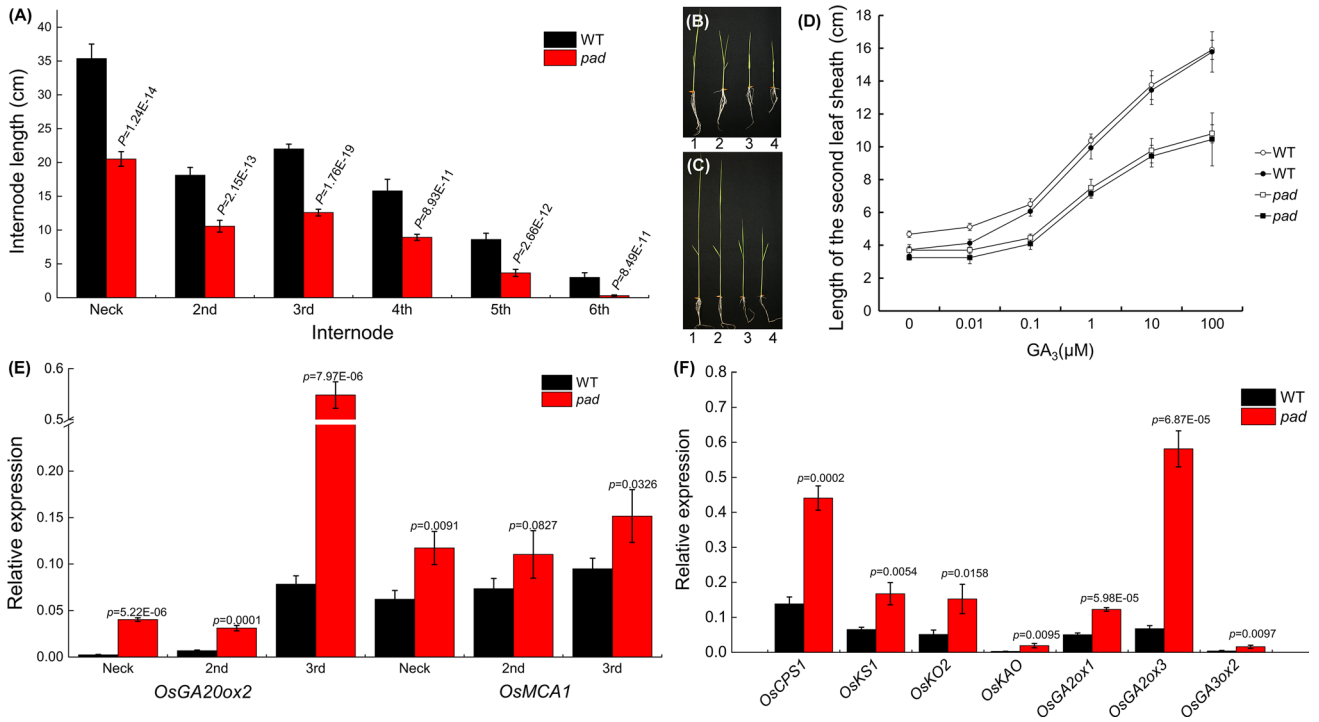

Fig. 7 Alterations in GA metabolism in *pad*. **a** Lengths of each internode in WT and *pad* plants. **b** Seedling phenotypes of WT (*1* and *2*) and the *pad* mutant (*3* and *4*) 8 days after germination. The seedlings were pretreated with (*2* and *4*) or without (*1* and *3*) 6.85 μM uniconazol on a 1 % agar plate without GA_3. **c** Seedling phenotypes of WT (*1* and *2*) and the *pad* mutant (*3* and *4*) 8 days after germination. The seedlings were pretreated with (*2* and *4*) or without (*1* and *3*) 6.85 μM uniconazol on a 1 % agar plate supplemented with 1 μM GA_3. **d** Second leaf sheath comparison between WT (*circle*) and *pad* (*square*) in response to GA treatment in seedlings pretreated with (*closed circles* and *closed squares*) or without (*open circles* and *open squares*) 6.85 μM uniconazol. **e** qRT-PCR analysis of *OsGA20ox2* and *OsMCA1/PAD* in the uppermost to third internodes of WT and *pad*. **f** qRT-PCR analysis of the genes involved in GA metabolism in the third internode of WT and *pad*. The data are given as the mean ± SD (n = 10) in (**a**) and (**d**). The mean ± SD were calculated from three biological replicates in (**e**) and (**f**). Values were determined by the Student's *t* test in (**a**) and (**e–f**)

Table 2 Contents of endogenous GAs in the third internode of WT plants and *pad* mutants (ng^{-1} g^{-1} FW)

	GA_{53}	GA_{44}	GA_{19}	GA_{20}	GA_1	GA_8	GA_{29}
WT	1.24 ± 0.02	0.51 ± 0.03	5.98 ± 0.55	0.20 ± 0.02	0.63 ± 0.01	ND	ND
pad	0.36 ± 0.01	0.25 ± 0.01	2.13 ± 0.08	0.13 ± 0.01	0.20 ± 0.01	0.17 ± 0.03	ND

The data are shown as the mean ± SD

ND not detected

pad mutant could involve in GA metabolism. To explore whether GA plays a role in the dwarf phenotype of the *pad* mutant, we first compared the effects of GA on shoot elongation in the mutant and WT. Sterilized WT and mutant seeds were pretreated with or without 6.85 μM uniconazol, an inhibitor of GA biosynthesis, and then placed on 1 % agar plates supplemented with GA_3 at concentrations ranging from 0.01 to 100 μM. By analyzing the length of the second leaf sheath after 8 days of treatment, we found that the *pad* mutant exhibited less sensitivity to exogenous GA_3 compared with WT irrespective of uniconazol pretreatment (Fig. 7b–d). Although the *pad* mutant exhibited insensitive to exogenous GA_3, it did respond to GA in a concentration-dependent manner.Furthermore, the difference in the length of the second sheath became more obvious with increasing GA_3 concentrations (Fig. 7d). Therefore, *OsMCA1/PAD* could be involved in regulating GA metabolism.

To determine whether there was a difference in GA content between WT and the mutant, we monitored endogenous GA levels in the early 13-hydroxylation pathway of GA metabolism in the third internode. In the *pad* mutant, the levels of the precursors of GA_1, GA_{53}, GA_{44} and GA_{19}, were reduced by approximately one-third to one-half compared with WT. In the *pad* mutant, bioactive GA (GA_1)

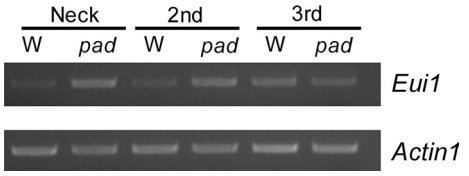

Fig. 8 Transcription level of *Eui1* of the uppermost to the third internodes in WT and *pad*. *Actin1* was used as the internal control

contents significantly decreased to less than one-third of WT levels (Table 2). To determine whether GA metabolism was regulated by *OsMCA1/PAD*, we analyzed the expression levels of genes involved in GA metabolism. The expression pattern of *OsGA20ox2,* the key gene involved in GA biosynthesis in rice, was similar to that of *OsMCA1/PAD* (Fig. 7e) and was significantly increased from the uppermost internode to the third internode in the mutant compared with WT. Moreover, other genes involved in GA biosynthesis, including *OsCPS1*, *OsKS1*, *OsKO2*, *OsKAO* and *OsGA3ox2*, were also up-regulated in the third internode of the *pad* mutant. Interestingly, the expression of GA deactivation genes *OsGA2ox1* and *OsGA2ox3* also significantly increased in the third internode of the *pad* mutant (Fig. 7f). These results suggest that *OsMCA1/PAD* may regulate GA biosynthesis and catabolism.

Furthermore, similar expression patterns of the genes involved in GA metabolism were also observed in the uppermost internode and second internode (Supplemental Fig. S4). Moreover, significant difference in the transcription levels of *Eui1* was also found in the uppermost internode and second internode between *pad* and the WT, while no significant difference between *pad* and the WT in the third internode (Fig. 8).

Taken together, these results indicated that the loss-of-function mutation in the *OsMCA1/PAD* led to upregulation of the expression of the genes related to GA deactivation, which decreased bioactive GA levels. As a consequence, the lower active GA contents could induce to constitutively upregulate the expression of the genes for GA biosynthesis by feedback regulation cycles, consequently, affecting plant architecture by inhibiting cell elongation.

Discussion

MCA1 genes are highly conserved in higher plants

Two *MCA1* homologs, *Mid1-Complementing Activity 1* (*AtMCA1*) and *Mid1-Complementing Activity 2* (*AtMCA2*), which encode plasma membrane proteins with mechanosensitive (MS) channel activity corresponding to Ca^{2+} uptake, have been reported in *Arabidopsis* (Nakagawa et al. 2007; Yamanaka et al. 2010). Increased *AtMCA1* expression can promote Ca^{2+} uptake in roots and elevate cytoplasmic free Ca^{2+} concentrations upon hypo-osmotic shock. Furthermore, the N terminus of both proteins contain EF hand-like domains and are indispensable for Ca^{2+} uptake (Nakano et al. 2011). In addition, *OsMCA1*, a rice homolog of *MCA* in *Arabidopsis*, also plays a critical role in Ca^{2+}-permeable mechanosensitive channel activity and participates in the regulation of reactive oxygen species (ROS) generation induced by hypo-osmotic stress in cultured rice cells (Kurusu et al. 2012). Phylogenetic tree analysis revealed that the OsMCA1/PAD homologous proteins group into two clades, one belonging to monocots and the other belonging to dicots. A putative uncharacterized protein encoded on chromosome 6, EEE65313.1 (*O. sativa*), shares 87 % sequence identity with OsMCA1/PAD (Supplemental Fig. S5). Even so, OsMCA1/PAD was described as a sole homolog of AtMCAs in the rice genome based on the genome data search (Kurusu et al. 2012). These data indicate that the OsMCA1/PAD protein may exhibit a highly conserved biological function in higher plants.

OsMCA1 is involved in the modulation of rice plant architecture

Previous studies have reported that the *MCA1* gene involved in calcium signaling in *Arabidopsis* and rice (Nakagawa et al. 2007; Nakano et al. 2011; Yamanaka et al. 2010) and fruit size in tomato (Frary et al. 2000). No reports have shown that *MCA1* affects plant architecture via regulating GA metabolism. In the present study, we isolated a natural *pad* mutant with defective plant architecture, including reduced plant height, a shorter root, stunted leaves, smaller panicles, fewer secondary branches, an altered number of spikelets per panicle and a lower seed rating compared with WT. Using qRT-PCR analysis and a GUS activity assay, we found that the *OsMCA1/PAD* gene is expressed in the majority of tissues during the vegetative and reproductive growth stages, which is consistent with the abnormal mutant phenotype. As a result, the combined mutant phenotypic characteristics could cause a reduction in grain yield.

Using a map-based cloning strategy and rescue assay, we confirmed that a point mutation in a single gene, *OsMCA1*, caused defects throughout the rice plant developmental stages. The genetic complementation experiment confirmed the *pad* is a loss-of-function mutation. This SNP was found in the kinase domain and converted a hydrophilic amino acid to a hydrophobic amino acid. A single amino acid change in the kinase domain led to major plant architecture defects, revealing that the *OsMCA1/PAD* gene involves in the regulation of plant architecture, which has not been reported previously. Further investigation demonstrated

that mutated *OsMCA1/PAD* affects cell size and cell elongation in leaves, stems and internodes. This result is inconsistent with results for the *OsMCA1/PAD* orthologs fw2.2 and cell number regulators (CNRs) in tomato and maize, which control plant organ size by regulating cell proliferation but not cell expansion (Cong et al. 2002; Frary et al. 2000; Guo et al. 2010). Our data show that a single SNP (R44P) might endow *OsMCA1/PAD* with a novel function in rice.

mOsMCA1 may have gained a novel biological function

Bioinformatics and subcellular localization analyses indicated that *OsMCA1/PAD* encodes a transmembrane protein and contains a putative STYKc domain, a conserved coiled–coil region and a PLAC8 motif. In addition, an EF hand-like domain adjacent to the ARPK domain of MCA1 has been predicated in *Arabidopsis* (Nakagawa et al. 2007; Nakano et al. 2011). The STYKc domain was described as a possible dual-specificity Ser/Thr/Tyr kinase domain based on the annotation in the SMART protein database. The specificity of this class of kinases cannot be predicted, and its function is poorly understood in rice. In *Arabidopsis*, the STYKc domain may be involved in mediating morphological alterations (Uchida et al. 2011), intercellular communication during meristem maintenance regulation and differentiation (Hattan et al. 2004) and the formation of normal epidermal surfaces during embryogenesis (Tsuwamoto et al. 2008). There is also some information regarding STYKc function in animals. As a novel effector caspase, the characteristic kinase domain STYKc may play a role in innate immunity in sponges (Wiens et al. 2007). Cyclin-dependent kinase 5 (cdk5)/p53-regulated kinase (cprk), which was characterized as a novel neuronal kinase, harbors a STYKc domain that has kinase activity and functions in the brain (Kesavapany et al. 2003). These researches have suggested that R44P in OsMCA1/PAD could affect the kinase activity of MCA1.

OsMCA1 involves in regulating GA deactivation

Previous studies have reported that *MCA1* is involved in calcium signaling and fruit size (Kurusu et al. 2012; Nakagawa et al. 2007; Yamanaka et al. 2010). However, our data show that *OsMCA1/PAD* affects plant architecture via regulating GA metabolism. Cytological studies indicated that internode elongation is regulated by the suppression of cell elongation. Compared with another classical GA-deficient rice mutant *sd1*, the *pad* was less responsive to exogenous GA_3 treatment than WT and the sheath length of *pad* was not completely recovered to that of the WT at 100 μM of GA_3 in seedling stage. While the sheath length of *sd1* was fully rescued under exogenous GA_3 treatment (Ashikari et al. 2002), implying that *OsMCA1/PAD* gene is distinct functions from *SD1*. Further analyses revealed that the key genes for GA biosynthesis, *OsGA20ox2* and *OsGA3ox2*, were upregulated in the uppermost to third internodes of *pad* mutant. The expression of *OsGA20ox2* in the *pad* mutant was significantly increased in the second and third internodes compared with WT, whereas higher expression was detected in the first internode of the *pad* mutant in contrast to the *d1* mutant (Ueguchi-Tanaka et al. 2000). In addition, endogenous GA levels generally decreased in the third internode of the *pad* mutant compared with WT. In contrast, higher GA levels accumulated in the third internode of the *d1* mutant. Moreover, we surprisingly observed that the expression of other genes involved in the GA biosynthesis and deactivation were upregulated. The expression profiles of those genes are highly correlated to the upregulation of *OsMCA1* expression in *pad* mutant. As shown in Supplemental Fig. S6, *Osmca1/pad* upregulated the expression of the genes for GA deactivation, such as *OsGA2ox1, OsGA2ox3 and Eui1,* leading to the significant decrease of bioactive GA contents in the third internode. As a consequence, the reduction of bioactive GA contents could induce to constitutively upregulate the expression of the genes for GA biosynthesis by feedback regulation cycles.

In summary, our results show that *OsMCA1/PAD* gene is responsible for the plant architecture defect. A SNP leads to an amino acid change R44P at a STYKc domain on N terminus of OsMCA1 and inhibits cell elongation. The loss-of-function of the *OsMCA1/PAD* leads to upregulation of gene expression related to GA deactivation and subsequent downregulation of bioactive GA levels to finally cause the plant dwarf phenotype. Therefore, *OsMCA1/PAD* may function as a positive regulator involved in plant growth and development. This finding will provide insight to further understanding of the mechanism of GA metabolism regulation and the function of kind of *OsMCA1/PAD* genes in higher plants.

Acknowledgments We thank Prof. Yu-Qi Feng for technical assistance of GA content analysis. This work was supported by the National Natural Science Foundation of China (No.3087496).

Conflict of interest The authors declare that they have no conflict of interest.

References

Ashikari M, Sasaki A, Ueguchi-Tanaka M, Itoh H, Nishimura A, Datta S, Ishiyama K, Saito T, Kobayashi M, Khush GS (2002) Loss-of-function of a rice gibberellin biosynthetic gene, *GA20 oxidase* (*GA20ox-2*), led to the rice 'green revolution'. Breed Sci 52:143–150

Chen ML, Fu XM, Liu JQ, Ye TT, Hou SY, Huang YQ, Yuan BF, Wu Y, Feng YQ (2012) Highly sensitive and quantitative profiling

of acidic phytohormones using derivatization approach coupled with nano-LC-ESI-Q-TOF-MS analysis. J Chromatogr B Analyt Technol Biomed Life Sci 905:67–74

Cong B, Liu J, Tanksley SD (2002) Natural alleles at a tomato fruit size quantitative trait locus differ by heterochronic regulatory mutations. Proc Natl Acad Sci USA 99:13606–13611

Dai M, Zhao Y, Ma Q, Hu Y, Hedden P, Zhang Q, Zhou DX (2007) The rice *YABBY1* gene is involved in the feedback regulation of gibberellin metabolism. Plant Physiol 144:121–133

Frary A, Nesbitt TC, Grandillo S, Knaap E, Cong B, Liu J, Meller J, Elber R, Alpert KB, Tanksley SD (2000) *fw2.2*: a quantitative trait locus key to the evolution of tomato fruit size. Science 289:85–88

Guo M, Rupe MA, Dieter JA, Zou J, Spielbauer D, Duncan KE, Howard RJ, Hou Z, Simmons CR (2010) *Cell Number Regulator1* affects plant and organ size in maize: implications for crop yield enhancement and heterosis. Plant Cell 22:1057–1073

Guo X, Hou X, Fang J, Wei P, Xu B, Chen M, Feng Y, Chu C (2013) The rice *GERMINATION DEFECTIVE 1*, encoding a B3 domain transcriptional repressor, regulates seed germination and seedling development by integrating GA and carbohydrate metabolism. Plant J 75:403–416

Hattan J, Kanamoto H, Takemura M, Yokota A, Kohchi T (2004) Molecular characterization of the cytoplasmic interacting protein of the receptor kinase IRK expressed in the inflorescence and root apices of *Arabidopsis*. Biosci Biotechnol Biochem 68:2598–2606

Hedden P, Thomas SG (2012) Gibberellin biosynthesis and its regulation. Biochem J 444:11–25

Huang J, Tang D, Shen Y, Qin B, Hong L, You A, Li M, Wang X, Yu H, Gu M, Cheng Z (2010) Activation of gibberellin 2-oxidase 6 decreases active gibberellin levels and creates a dominant semi-dwarf phenotype in rice (*Oryza sativa* L.). J Genet Genomics 37:23–36

Ikeda A, Ueguchi-Tanaka M, Sonoda Y, Kitano H, Koshioka M, Futsuhara Y, Matsuoka M, Yamaguchi J (2001) *slender* rice, a constitutive gibberellin response mutant, is caused by a null mutation of the SLR1 gene, an ortholog of the height-regulating gene *GAI*/*RGA*/*RHT*/*D8*. Plant Cell 13:999–1010

Itoh H, Tatsumi T, Sakamoto T, Otomo K, Toyomasu T, Kitano H, Ashikari M, Ichihara S, Matsuoka M (2004) A rice semi-dwarf gene, *Tan-Ginbozu* (*D35*), encodes the gibberellin biosynthesis enzyme, *ent*-kaurene oxidase. Plant Mol Biol 54:533–547

Jefferson RA (1989) The GUS reporter gene system. Nature 342:837–838

Jiao Y, Wang Y, Xue D, Wang J, Yan M, Liu G, Dong G, Zeng D, Lu Z, Zhu X, Qian Q, Li J (2010) Regulation of *OsSPL14* by OsmiR156 defines ideal plant architecture in rice. Nat Genet 42:541–544

Jin J, Huang W, Gao JP, Yang J, Shi M, Zhu MZ, Luo D, Lin HX (2008) Genetic control of rice plant architecture under domestication. Nat Genet 40:1365–1369

Kesavapany S, Lau KF, Ackerley S, Banner SJ, Shemilt SJ, Cooper JD, Leigh PN, Shaw CE, McLoughlin DM, Miller CC (2003) Identification of a novel, membrane-associated neuronal kinase, cyclin-dependent kinase 5/p35-regulated kinase. J Neurosci 23:4975–4983

Kurusu T, Nishikawa D, Yamazaki Y, Gotoh M, Nakano M, Hamada H, Yamanaka T, Iida K, Nakagawa Y, Saji H, Shinozaki K, Iida H, Kuchitsu K (2012) Plasma membrane protein OsMCA1 is involved in regulation of hypo-osmotic shock-induced Ca_2^+ influx and modulates generation of reactive oxygen species in cultured rice cells. BMC Plant Biol 12:11

Li X, Qian Q, Fu Z, Wang Y, Xiong G, Zeng D, Wang X, Liu X, Teng S, Hiroshi F, Yuan M, Luo D, Han B, Li J (2003) Control of tillering in rice. Nature 422:618–621

Li P, Wang Y, Qian Q, Fu Z, Wang M, Zeng D, Li B, Wang X, Li J (2007) *LAZY1* controls rice shoot gravitropism through regulating polar auxin transport. Cell Res 17:402–410

Magome H, Nomura T, Hanada A, Takeda-Kamiya N, Ohnishi T, Shinma Y, Katsumata T, Kawaide H, Kamiya Y, Yamaguchi S (2013) *CYP714B1* and *CYP714B2* encode gibberellin 13-oxidases that reduce gibberellin activity in rice. Proc Natl Acad Sci USA 110:1947–1952

Miura K, Ikeda M, Matsubara A, Song XJ, Ito M, Asano K, Matsuoka M, Kitano H, Ashikari M (2010) *OsSPL14* promotes panicle branching and higher grain productivity in rice. Nat Genet 42:545–549

Nakagawa Y, Katagiri T, Shinozaki K, Qi Z, Tatsumi H, Furuichi T, Kishigami A, Sokabe M, Kojima I, Sato S, Kato T, Tabata S, Iida K, Terashima A, Nakano M, Ikeda M, Yamanaka T, Iida H (2007) *Arabidopsis* plasma membrane protein crucial for Ca_2^+ influx and touch sensing in roots. Proc Natl Acad Sci USA 104:3639–3644

Nakano M, Iida K, Nyunoya H, Iida H (2011) Determination of structural regions important for Ca(2+) uptake activity in Arabidopsis MCA1 and MCA2 expressed in yeast. Plant Cell Physiol 52:1915–1930

Olszewski N, Sun TP, Gubler F (2002) Gibberellin signaling: biosynthesis, catabolism, and response pathways. Plant Cell 14(Suppl):S61–S80

Sakamoto T (2006) Phytohormones and rice crop yield: strategies and opportunities for genetic improvement. Transgenic Res 15:399–404

Sakamoto T, Matsuoka M (2004) Generating high-yielding varieties by genetic manipulation of plant architecture. Curr Opin Biotechnol 15:144–147

Sakamoto T, Miura K, Itoh H, Tatsumi T, Ueguchi-Tanaka M, Ishiyama K, Kobayashi M, Agrawal GK, Takeda S, Abe K, Miyao A, Hirochika H, Kitano H, Ashikari M, Matsuoka M (2004) An overview of gibberellin metabolism enzyme genes and their related mutants in rice. Plant Physiol 134:1642–1653

Sakamoto T, Morinaka Y, Ohnishi T, Sunohara H, Fujioka S, Ueguchi-Tanaka M, Mizutani M, Sakata K, Takatsuto S, Yoshida S, Tanaka H, Kitano H, Matsuoka M (2006) Erect leaves caused by brassinosteroid deficiency increase biomass production and grain yield in rice. Nat Biotechnol 24:105–109

Sasaki A, Ashikari M, Ueguchi-Tanaka M, Itoh H, Nishimura A, Swapan D, Ishiyama K, Saito T, Kobayashi M, Khush GS, Kitano H, Matsuoka M (2002) Green revolution: a mutant gibberellin-synthesis gene in rice. Nature 416:701–702

Springer N (2010) Shaping a better rice plant. Nat Genet 42:475–476

Takeda K (1979) Internode elongation and dwarfism in some gramineous plants. Gamma field symp 16:1–18

Takeda T, Suwa Y, Suzuki M, Kitano H, Ueguchi-Tanaka M, Ashikari M, Matsuoka M, Ueguchi C (2003) The *OsTB1* gene negatively regulates lateral branching in rice. Plant J 33:513–520

Tan L, Li X, Liu F, Sun X, Li C, Zhu Z, Fu Y, Cai H, Wang X, Xie D, Sun C (2008) Control of a key transition from prostrate to erect growth in rice domestication. Nat Genet 40:1360–1364

Thomas SG, Rieu I, Steber CM (2005) Gibberellin metabolism and signaling. Vitam Horm 72:289–338

Tsuwamoto R, Fukuoka H, Takahata Y (2008) *GASSHO1* and *GASSHO2* encoding a putative leucine-rich repeat transmembrane-type receptor kinase are essential for the normal development of the epidermal surface in *Arabidopsis* embryos. Plant J 54:30–42

Uchida N, Igari K, Bogenschutz NL, Torii KU, Tasaka M (2011) Arabidopsis ERECTA-family receptor kinases mediate morphological alterations stimulated by activation of NB-LRR-type UNI proteins. Plant Cell Physiol 52:804–814

Ueguchi-Tanaka M, Fujisawa Y, Kobayashi M, Ashikari M, Iwasaki Y, Kitano H, Matsuoka M (2000) Rice dwarf mutant *d1*, which is defective in the alpha subunit of the heterotrimeric G protein, affects gibberellin signal transduction. Proc Natl Acad Sci USA 97:11638–11643

Wang Y, Li J (2005) The plant architecture of rice (*Oryza sativa*). Plant Mol Biol 59:75–84

Wang Y, Li J (2008) Rice, rising. Nat Genet 40:1273–1275

Wiens M, Korzhev M, Perovic-Ottstadt S, Luthringer B, Brandt D, Klein S, Muller WE (2007) Toll-like receptors are part of the innate immune defense system of sponges (demospongiae: porifera). Mol Biol Evol 24:792–804

Wu X, Tang D, Li M, Wang K, Cheng Z (2013) Loose Plant Architecture1, an INDETERMINATE DOMAIN protein involved in shoot gravitropism, regulates plant architecture in rice. Plant Physiol 161:317–329

Xing Y, Zhang Q (2010) Genetic and molecular bases of rice yield. Annu Rev Plant Biol 61:421–442

Yamaguchi S (2008) Gibberellin metabolism and its regulation. Annu Rev Plant Biol 59:225–251

Yamanaka T, Nakagawa Y, Mori K, Nakano M, Imamura T, Kataoka H, Terashima A, Iida K, Kojima I, Katagiri T, Shinozaki K, Iida H (2010) MCA1 and MCA2 that mediate Ca_2^+ uptake have distinct and overlapping roles in Arabidopsis. Plant Physiol 152:1284–1296

Yang XC, Hwa CM (2008) Genetic modification of plant architecture and variety improvement in rice. Heredity 101:396–404

Yoshihara T, Iino M (2007) Identification of the gravitropism-related rice gene *LAZY1* and elucidation of LAZY1-dependent and -independent gravity signaling pathways. Plant Cell Physiol 48:678–688

Yu B, Lin Z, Li H, Li X, Li J, Wang Y, Zhang X, Zhu Z, Zhai W, Wang X, Xie D, Sun C (2007) *TAC1*, a major quantitative trait locus controlling tiller angle in rice. Plant J 52:891–898

Zhang Q, Li J, Xue Y, Han B, Deng XW (2008) Rice 2020: a call for an international coordinated effort in rice functional genomics. Mol Plant 1:715–719

Zhu Y, Nomura T, Xu Y, Zhang Y, Peng Y, Mao B, Hanada A, Zhou H, Wang R, Li P, Zhu X, Mander LN, Kamiya Y, Yamaguchi S, He Z (2006) *ELONGATED UPPERMOST INTERNODE* encodes a cytochrome P450 monooxygenase that epoxidizes gibberellins in a novel deactivation reaction in rice. Plant Cell 18:442–456